THE INFLUENCE OF THE SUBSTRATE TEMPERATURE ON THE PHISICOCHEMICAL PROPERTIES OF CALCIUM PHOSPHATE LAYERS DEPOSITED BY LOW POWER RADIO-FREQUENCY MAGNETRON SPUTTERING DISCHARGE

Maria-Elena ZARIF[1,2], Andreea GROZA[1], Sasa Alexandra YEHIA-ALEXE[1,3], Bogdan BITA[1,3], Ecaterina ANDRONESCU[2,4,5,*]

In this study we report the deposition of calcium phosphate layers by Radio-Frequency Magnetron Sputtering technique at 50 W low power and a target-to-substrate distance of about 8 cm, when the substrate temperature was externally controlled from 25 to 200 ℃. The scanning electron microscopy investigations of the surface morphologies of the layers obtained when the substrates were externally heated indicated the formation of compact microcavities. The Ca/P atomic ratios were 1.8 for all coatings. The Fourier transform infrared spectra peak fitting analysis indicated that the peak area percentages vary as a function of the substrate temperature, revealing the molecular changes in the layers. The X-ray photoelectron spectroscopy investigation confirmed that the surface chemistry is dependent on the deposition conditions.

Keywords: calcium phosphates, radio frequency magnetron sputtering.

1. Introduction

The radio-frequency magnetron sputtering (RF-MS) technique is used for the deposition of calcium phosphates (CaPs) coatings due to the fact that it ensures a good adhesion of the layers to the substrate and a good control of their properties, including the Ca/P atomic ratio [1]. The properties of the coatings are dependent on several factors such as the RF power [2], the working pressure [3], the deposition time [2,4], the substrate temperature [5–7], the sputtering target material [7,8] (e.g., hydroxyapatite (HAp), tricalcium phosphate (TCP), dicalcium phosphate (DCP), or other CaPs, their mixture, or doped CaPs), and the substrate type [6,7] (e.g. Si or

[1] National Institute for Lasers, Plasma and Radiation Physics, Măgurele, Romania
[2] Faculty of Chemical Engineering and Biotechnologies, The National University of Science and Technology POLITEHNICA Bucharest, Romania
[3] Faculty of Physics, University of Bucharest, Măgurele, Romania
[4] Academy of Romanian Scientists, Bucharest, Romania
[5] National Research Center for Micro and Nanomaterials, The National University of Science and Technology POLITEHNICA Bucharest, Romania
*Correspondence: ecaterina.andronescu@upb.ro

Ti). Our previous results indicated that layers synthetized from sputtering HAp targets have Ca/P atomic ratios dependent on the substrate temperature when the coatings were deposited on Ti substrates [5,7]. In the case of Sr-doped HAp sputtering targets, the (Ca+Sr)/P atomic ratios were equal in the case of the layers generated on Si samples and slightly decreased with the substrate temperature increase when deposited on mirror-like Ti substrates [6,7].

The coatings deposited by RF-MS are generally amorphous and additionally annealing is required to increase the crystallinity of the layers [9]. It has been reported that the Ca/P atomic ratios of as-deposited RF-MS generated layers is lower than the Ca/P atomic ratios of the corresponding targets, but increase above these values after annealing [8,9]. Boyd et al. [9] reported that for thermally-treated layers deposited using a three sputtering target system of HAp, TCP, or two targets of HAp and one of DCP, semi-crystalline HAp-like coatings are obtained, with Ca/P atomic ratios of 1.82, 1.73, and 1.43, respectively. These rations were higher than those corresponding to the as-deposited layers, which were 1.35, 1.23, and 1.19, respectively. Similar results regarding the evolution of Ca/P atomic ratios of the CaPs layers before and after annealing were reported by O'Kane et al. [8]. The amorphous nature of the as-deposited layers was evidenced by poorly defined peaks in the Fourier Transform Infrared Spectroscopy (FTIR) spectra [8]. The FTIR investigation can indicate the beginning of crystallization for the CaPs by narrower ν_3 bands and splitted ν_4 bands, characteristic for the triply degenerated antisymmetric stretching mode of P-O bonds and triply degenerated antisymmetric bending mode of O-P-O bonds, respectively [10]. Besides these, two other absorption bands in the FTIR spectra, characteristic for the non-degenerated symmetric stretching mode of P-O (ν_1) and for the symmetric out-of-plane bending of O-P-O (ν_2), are also an indication of the phosphate group [10]. Generally, additional steps, such as annealing, are to be avoided. Therefore, the externally heating of the substrate during the physical vapor deposition could be a solution.

In this regard, the aim of this study is to evidence the impact of the substrate temperature on the physicochemical properties of CaPs layers generated by RF-MS at low power. The research of RF-MS generated CaP layers was generally focused on short (up to 4-5 cm) target-to-substrate distances [2,4,11–22]
and/or high powers, usually above 100 W [2,4,8,9,11–15,23–28] to ensure coatings with improved crystallinity and high thicknesses. However, for heat-sensitive substrates such conditions cannot be used. Therefore, this study represents the first step into the evaluation of the development of this technique for the deposition of CaP layers on heat-sensitive substrates or from organic-CaP composite sputtering targets.

2. Materials and methods

Sputtering targets (diameter: 5 cm; thickness: ~ 4 mm) were obtained by pressing a calcium phosphate (CaP) tribasic powder [$Ca_{10}(OH)_2(PO_4)_6$; CAS number: 12167-74-7; Alfa Aesar]. The CaP layers were deposited on Ti substrates with a mirror-like surface.

The CaP coatings were synthetized in the following conditions: 50 W RF power, 10 h deposition time, and substrate temperatures of 25, 100 and 200 °C. These temperatures were measured before starting of the RF-MS discharge using a single ended thermocouple probe. The heating of the substrates was done using a homemade oven. It must be mentioned that the substrate temperatures increase above these values during the CaP deposition due to plasma heating. For an initial substrate temperature of 25 °C, after 10 h deposition time, the substrate temperature reaches ~120 °C. Considering this, the highest substrate temperature should not exceed ~320 °C. Details on the experimental equipment and other working parameters are presented in ref. [5] and listed in Table 1.

Table 1

Working parameters during the RF-MS deposition

Working parameter	Value
Power	50 W
Deposition time	10 h
Substrate temperature	25, 100, and 200 °C
Target-to-substrate distance	~8 cm
Base pressure	~10^{-5} mbar
Working pressure	~10^{-2} mbar
Gas	Ar
Gas flow	5 ml_n/min

A quartz crystal microbalance (INFICON Holding AG Company) was used to measure the deposition rate for the CaP layers, which was ~0.03 Å/s, resulting in a film thickness of around 100 nm.

The coatings were investigated by surface analysis methods such as Scanning Electron Microscopy (SEM) and X-Ray Photoelectron Spectroscopy (XPS). The elemental and molecular analysis of the CaP layers have been conducted by Energy Dispersive X-Ray Spectroscopy (EDX) and Fourier Transform Infrared Spectroscopy (FTIR).

SEM and EDX measurements have been performed using a ThermoFisher Apreo S scanning electron microscope and a SiLi EDX detector, at acceleration voltages of 8 and 10 kV, respectively.

The ATR-FTIR analysis revealed the features of CaPs molecular bands and was recorded with a Perkin-Elmer SP 100 FTIR spectrometer with a 4 cm^{-1} resolution in the range of 4000-400 cm^{-1}. Through the SPECTRUM software of the

FTIR spectrometer the transmission spectra were converted into absorption one. Due to the fact that the absorption bands in the FTIR spectra were not well resolved, the peak fitting analysis was required to identify the overlapping bands. In this regard, the 2nd order derivative analysis (OriginPro software) was required to identify the wavenumbers of these peaks. The MagicPlotPro software was used to perform the deconvolution procedure, using Lorentz fitting curves. The FWHMs were not limited during the peak fitting analysis. Only the wavenumber positions of the peaks were restricted to match the values observed from the 2nd order derivative analysis. The fitting results revealed that the RSS (X^2 - Residual sum of squares, also known as chi-squared) parameter was ranged between 0.0085 and 0.232 and that the coefficient of determination (R^2) was above 0.99 for all the peak fitting analysis.

The XPS allowed the evaluation of the chemical bonds at the CaP layer surfaces. The survey and the high-resolution XPS spectra were acquired using a K-Alpha Thermo Scientific (ESCALAB™ XI) spectrometer, with a monochromatic Al Kα source. All spectra were calibrated to the main line of C 1s at 284.6 eV to ensure the charge correction.

3. Results and discussion

3.1. Scanning Electron Microscopy

The morphology of the CaP/Ti layer surfaces is exhibited in Fig. 1. The SEM images indicated that compact areas and microcavities (Fig. 1 c and d) are formed at the surface of the coatings generated at 100 and 200 °C substrate temperatures. The morphology of the layers deposited at 25 °C substrate temperature is preponderantly porous (Fig. 1 b).

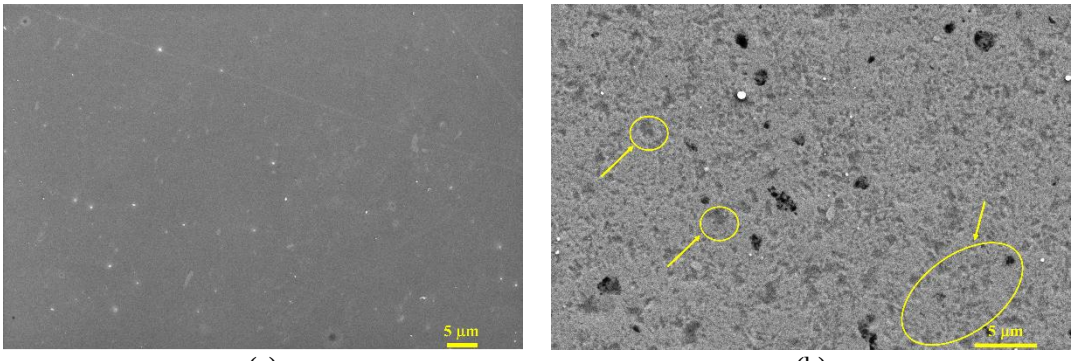

(a) (b)

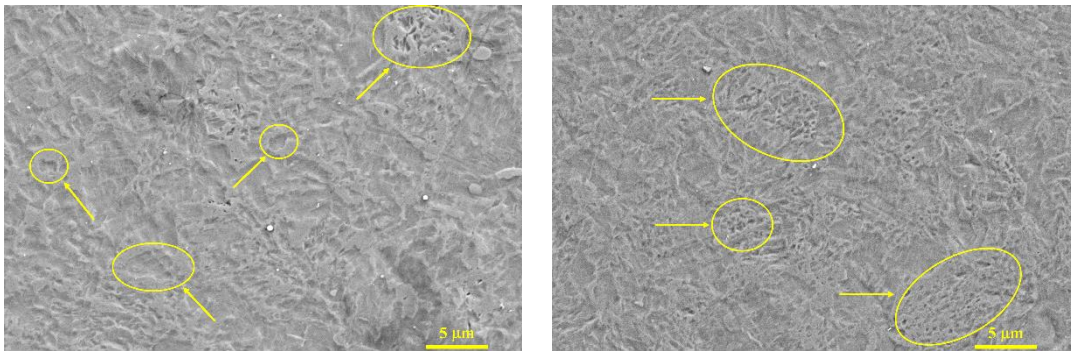

(c) (d)

Fig 1. SEM images of the (a) Ti substrate and of the CaP/Ti layers produced at the temperatures of the substrates of: (b) 25 °C, (c) 100 °C, and (d) 200 °C.

Our previous results [5], reported in the case of CaP/Ti layers produced at 100 W for 5 h, revealed that an increased substrate holder temperature in RF-MS discharge significantly changes the morphology of the surface from grain-like structures (25 °C) to more compact surfaces with microcavities (300 °C). At a substrate temperature of 300 °C [5], the surface morphology of the layers was similar for the following deposition parameters: 100 W for 5 h and 50 W for 10 h. It results that longer deposition times at low powers can provide the same surface characteristics of CaP/Ti layers when the substrate holder is externally heated at 300 °C.

The CaP layers deposited by RF-MS without increasing the substrate temperature with an external heating source (e.g. oven) have columnar growth, resulting in a grain-like surface morphology [15,29]. We assume that, as the substrate temperature increases, the coalescence of the grains appears, resulting in more compact layers and microcavities formation at their surface.

3.2. Energy-Dispersive X-Ray Spectroscopy

In the EDX spectrum of the substrate, titanium and nitrogen were identified (see Fig. 2 a). The EDX spectra of CaP/Ti layers (see Fig. 2 b, c, d) exhibit the Ca, P, and O characteristic elements. The Ca/P atomic ratios were 1.8 for all samples. This finding indicates that the layers may be composed out of amorphous CaPs and/or a mixture of CaPs phases. The Ca/P atomic ratios are higher than the stoichiometric ratio of HAp. This can be associated with the presence of CaO in the RF-MS generated layers [18], may suggest B-type carbonation, or may be assigned to the versatility of this ratio for HAp during the transition from an amorphous to a crystalline phase.

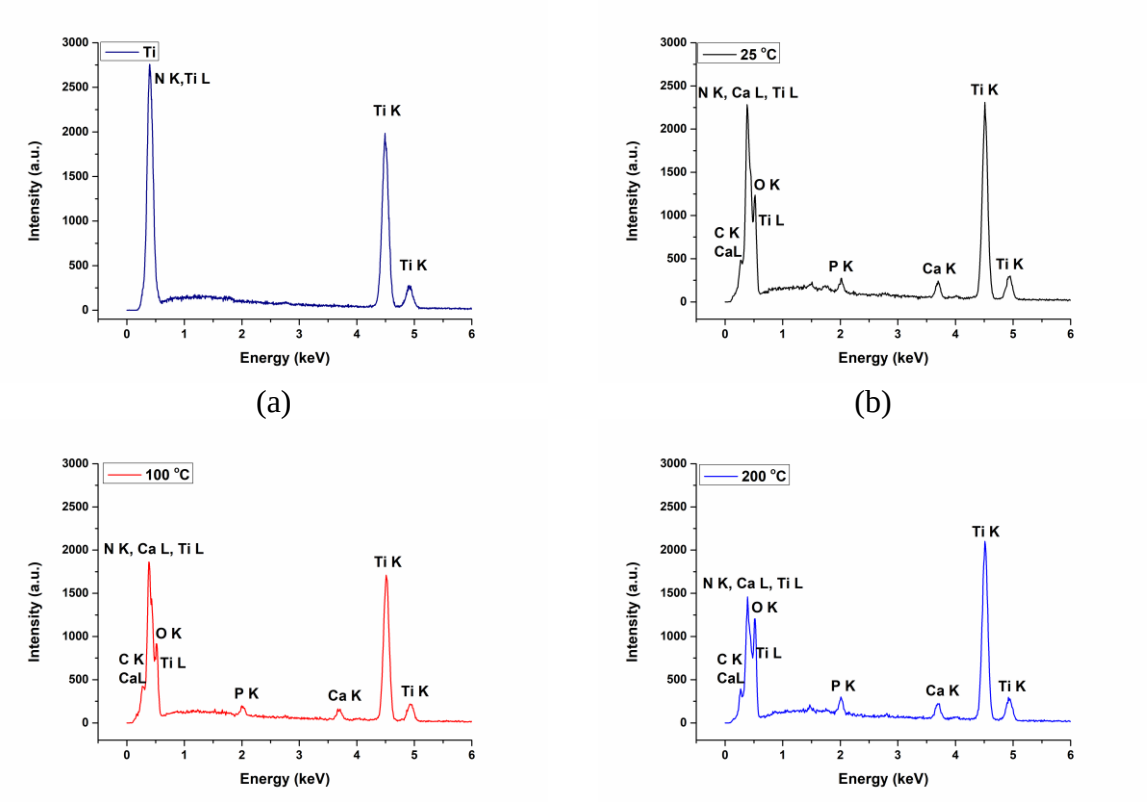

Fig. 2. EDX spectra of the (a) Ti substrate and CaP layers deposited at different substrate temperatures: (b) 25 °C, (c) 100 °C, and (d) 200°C.

3.3. Fourier Transform Infrared Spectroscopy

The CaP layers deposited by RF-MS are usually amorphous. This can be observed in the FTIR spectra by broad and non-split absorption bands characteristic for the phosphate group. The amorphous nature of such layers can also be revealed by the absence of the stretching (~3570 cm^{-1}) and libration (~630 cm^{-1}) modes of the structural hydroxyl. Therefore, the crystalline quality of the layers has been discussed considering the above-mentioned aspects, especially on the narrowing and the splitting of the absorbance bands characteristic for the phosphate group.

The FTIR spectra of the CaP/Ti layers produced at different temperatures of the substrate are presented in Fig. 3.

In the 4000-2000 cm^{-1} wavenumber range (Fig. 3. a), a broad absorption band can be observed. A broad absorption band in the 3600-2600 cm^{-1} wavenumber range can be attributed to adsorbed water.

For the layer deposited at a substrate temperature of 200 °C, a sharp and low intensity band can be observed at 3569 cm^{-1}, associated with the stretching

vibration mode of O-H bonds, indicating structural OH groups [30]. For this deposition condition, three low intensity absorption bands at 2962, 2920, and 2851 cm^{-1} were also identified in the FTIR spectrum and were associated with the stretching vibrations of C-H bonds [31]. The bands at 2962 and 2920 cm^{-1} were also identified in the FTIR spectrum of the layers deposited at 100 °C. These bands can be associated to ethanol, which has been used for the substrate cleaning before starting of the CaP layer deposition. We assume that the broadness of this band extends to 2000 cm^{-1} due to absorbed CO_3^{2-} [30]. However, the broadness of this band can also be associated to the O-H stretching vibration of HPO_4^{2-}, which appears in the FTIR spectrum within the wavenumber range 3400-2000 cm^{-1} [32,33].

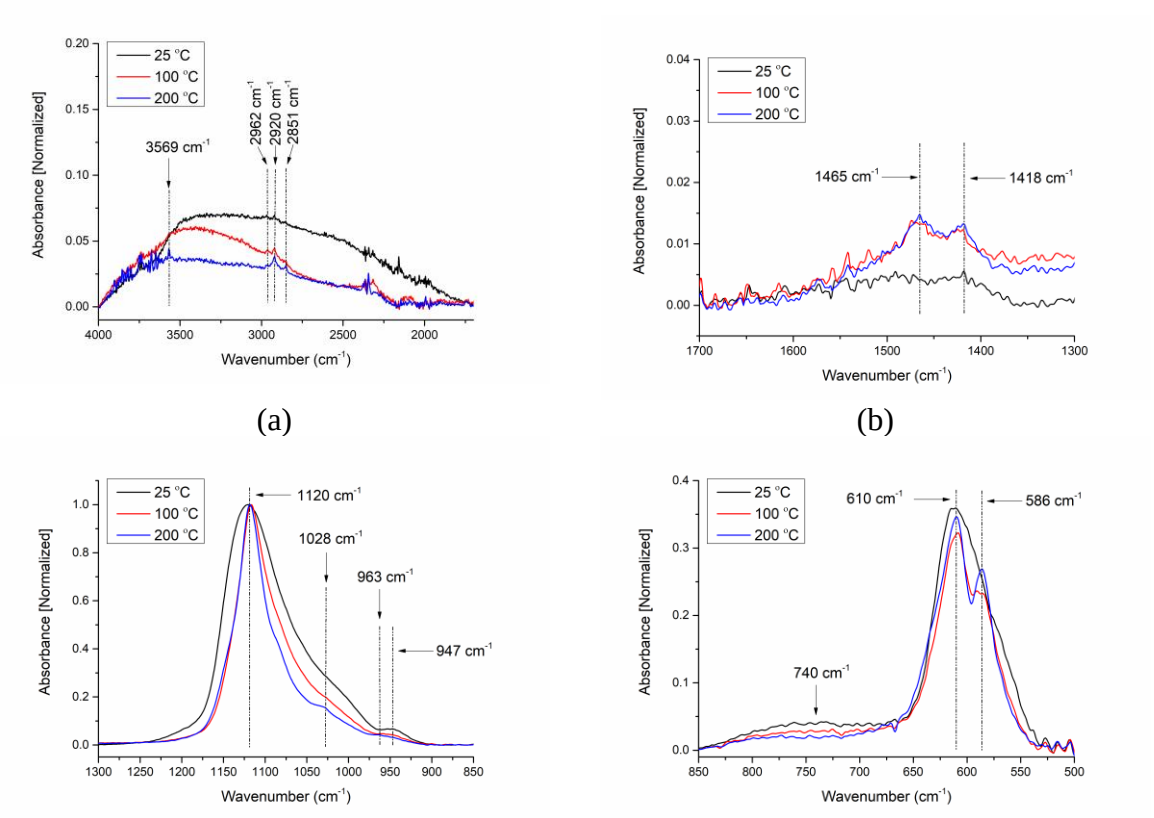

Fig. 3. FTIR spectra of the CaP layers in the wavenumber ranges of: (a) 4000-1700 cm^{-1}, (b) 1700-1300 cm^{-1}, (c) 1300-850 cm^{-1}, and (d) 850-500 cm^{-1}.

The absorption bands at 1465 and 1418 cm^{-1} (Fig. 3. b) are characteristic for the v_3 vibrations of the CO_3 group. The carbonate ion can substitute either the hydroxyl ion resulting, in A-type carbonated HAp, or the phosphate ion, resulting in B-type carbonated HAp. When both ions are substituted, there is an AB-type

substitution. The FTIR spectra of the CaP layers (Fig. 3. b) may suggest that B-type carbonation occurs [34–36], which could also explain the increase of the Ca/P atomic ratios. However, considering that these bands are very weak and the fact that in the wavenumber range 890-850 cm^{-1} the absorption band characteristic for the ν_2 vibration of the CO_3 group [35] was not observed, the carbonation of the CaP layers is very reduced.

In the 1300-900 cm^{-1} spectral range, the FTIR molecular bands are narrower as the substrate temperature increases. For the CaP deposited at 25 °C (Fig. 3, black line), the absorption band at ~ 1120 cm^{-1} is characteristic to P-O vibration in non-apatitic phosphate group [17,30,37,38] and/or to P-O-H in HPO_4^{2-} groups [25,39]. O'Kane et al. [8] reported the deposition of CaP thin films by RF-MS from HAp, α-TCP, and DCP sputtering targets. After annealing, a very strong absorption band, characteristic for the asymmetric stretching of the phosphate group, was identified at 1121 cm^{-1} for the layer deposited from a HAp sputtering target [8]. Strong IR peaks, characteristic to HPO_4^{2-} ions, namely P-O-H bond vibrations, were previously identified at 1120 and 580 cm^{-1} [25], 1126 and 582 cm^{-1} [9] by Boyd et al. and around 1117 and 584 cm^{-1} by Robinson et al. [39] for annealed coatings deposited from HAp sputtering targets. In their study, Robinson et al. [39] reported only a very weak shoulder around 875 cm^{-1}, which was not observed in the FTIR spectra of the layers investigated in our work (Fig. 3 c). The shifts between the absorbance bands of the coatings deposited at a substrate temperature of 100 °C (Fig. 3, red line) and 200 °C (Fig. 3, blue line) are under the FTIR resolution of 4 cm^{-1}: 1117 cm^{-1} and 1118 cm^{-1}, respectively and can be attributed to the vibrations in PO_4^{3-} and/or HPO_4^{2-} groups.

A shoulder at 1028 cm^{-1}, characteristic for the ν_3 vibrational mode of PO_4^{3-} in hydroxyapatite [5], was identified in the FTIR spectrum of the CaP layer deposited at a substrate temperature of 200 °C (Fig. 3, blue line).

Differences between the ν_1 symmetric stretching vibrational mode of PO_4^{3-} [30] of the layers deposited at 100 °C and 200 °C and the layer deposited without heating the substrate were observed. The wavenumbers were ~ 963 cm^{-1} (Fig. 3 red and blue lines) and 947 cm^{-1} (Fig. 3 black line), respectively. The absorption band at ~740 cm^{-1} is characteristic for $P_2O_7^{4-}$ [6]. The stretching modes of $P_2O_7^{4-}$ were previously identified at 726 and 1136 cm^{-1} [40] or 725 and 1215 cm^{-1} [9].

In the 700-500 cm^{-1} wavenumber range, a splitting of the absorption bands assigned to the ν_4 bending vibrational mode of PO_4^{3-} was observed for the coatings deposited by heating the substrates during the RF-MS deposition, with maximums at 610 cm^{-1} and 586 cm^{-1} (Fig 3. red and blue line). This split was not observed for the layer deposited without heating the substrate (Fig. 3 black line). The band at 586 cm^{-1} can be assigned to P-O vibrations in HPO_4^{2-} [39].

The narrowing of the ν_3 band and the splitting of the ν_4 band may indicate the beginning of crystallization, as previously reported by Uskoković [10].

Considering the broad absorption bands from the FTIR spectra of the CaP/Ti layers (Fig. 3), peak fitting analysis was required. The deconvolution results in the 1300-900 cm^{-1} and 700-500 cm^{-1} ranges are shown in Fig. 4 and summarized in Tables 2,3.

In the 1300-900 cm^{-1} range, for the layer deposited without heating the substrate (Fig. 4 a), the presence of $P_2O_7^{4-}$/P-OH was revealed by the 1136 cm^{-1} absorption band [8,40]. When the substrate temperature during the RF-MS discharge was increased, this absorption band was not further observed (Fig. 4 c and e and Table 1). This fact reveals that during the plasma deposition, the formation of pyrophosphate $P_2O_7^{4-}$ group is favored by a lower substrate temperature. Previously, we reported [5] the deposition of CaP layers on Ti substrates at a working power of 100 W for 5 h. The presence of $P_2O_7^{4-}$ group was not identified after the peak fitting analysis, highlighting therefore a different composition of the layers based on these two parameters.

The peak area percentage of the FTIR band at 1120 cm^{-1} (Fig. 4 a), assigned to PO_4^{3-} and/or HPO_4^{2-} group [17,30,37,38] increases from 12 % up to 64 %, as a function of substrate temperature (Table 2). The 1144 cm^{-1} peak was also assigned to HPO_4^{2-} [9].

The peak at 1098 cm^{-1} (Fig. 4 a, Table 2), assigned to ν_3 of PO_4^{3-} [5], shifted to lower wavenumbers, 1083 cm^{-1}, as the substrate temperature was increased and the area percentage decreased from 39 % to 20 % (Fig. 4 c and e, Table 2). The peak at 1055 cm^{-1}, completely disappeared from the FTIR spectrum of the CaP layer deposited at 100 and 200 °C (Fig. 4 e, Table 2). These results highlight that, as the substrate temperature is increased, the chemistry of the layers is changed, most probably due to the presence of different CaP phases.

Table 2

FTIR absorption bands assignments for the CaP layers deposited at different substrate temperatures and their peak area percentages in the 1300 – 900 cm^{-1} wavenumber range

Substrate temperature (°C)	**Wavenumber [cm^{-1}] (Peak Area Percentage)**					
	$P_2O_7^{4-}$/ P-OH	**HPO_4^{2-} and/or PO_4^{3-}**	**ν_3 of PO_4^{3-}** [41]			**ν_1 of PO_4^{3-}**
25	1136 (26 %)	1120 (12 %)	1098 (39 %)	1055 (11 %)	1024 (11 %)	946 (< 1 %)
100	-	1118 (58 %)	1083 (30 %)	-	1026 (11 %)	951 (< 1 %)
200	-	1118, 1144 (64 %, 4%)	1083 (20 %)	-	1028 (11 %)	963 (< 1 %)

Regarding the study of the ν_4 PO_4^{3-} domain, characteristic for the triply degenerated antisymmetric bending mode of O-P-O bonds, Christian Ray et al. [42]

are pioneers. In 1990, they demonstrated the presence of non-apatitic domains in HAp [42]. The deconvolution of this wavenumber domain, which is required for the investigation of poorly crystalline HAps, can highlight the presence of apatitic and non-apatitic PO_4^{3-} and HPO_4^{2-}, and of apatitic OH^- ions [43,44].

In the 700-500 cm^{-1} spectral range, the absorption bands around 617 cm^{-1} (Fig 4 b, d, and f, Table 3) were assigned to non-apatitic PO_4^{3-} [43] while the one at 554 cm^{-1} can be assigned either to PO_4^{3-} [30] or $P_2O_7^{4-}$ [9] (Fig. 4 b, Table 3).

The absorption band at 630 cm^{-1}, characteristic to the OH^- libration mode, is shifted to 634 cm^{-1} at a substrate temperature of 200 °C. For the layer deposited without heating the substrate, the peak area percentage is lower (Table 3), 8 %, probably due to the $P_2O_7^{4-}$ group. When the temperature at the substrate increases, the peak area percentage of non-apatitic PO_4^{3-} group decreases and the one characteristic to OH^- group inside HAp structure increases.

Table 3

FTIR absorption bands assignments for the CaP layers deposited at different substrate temperatures and their peak area percentages in the spectral range of 700 – 500 cm^{-1}

Substrate temperature (°C)	Wavenumber [cm^{-1}] (Peak Area Percentage)					
	ν_L OH^-	Non-apatitic PO_4^{3-}	PO_4^{3-}	HPO_4^{2-}	PO_4^{3-}	
25	630 (8 %)	617 (30 %)	602 (32 %)	585 (18 %)	568 (10 %)	554 (2 %)
100	630 (11 %)	617 (20 %)	606 (33 %)	584 (32 %)	567 (4 %)	-
200	634 (14 %)	619 (19%)	608 (33 %)	585 (31 %)	568 (3 %)	-

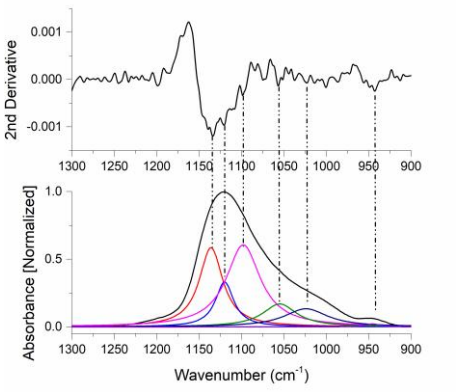

(a)

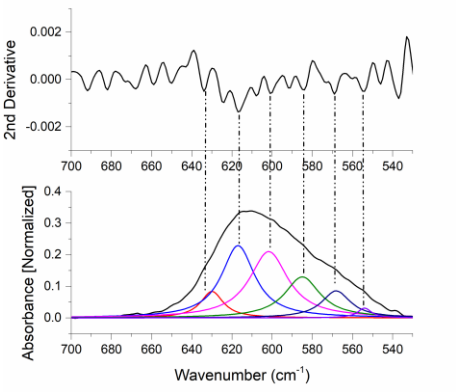

(b)

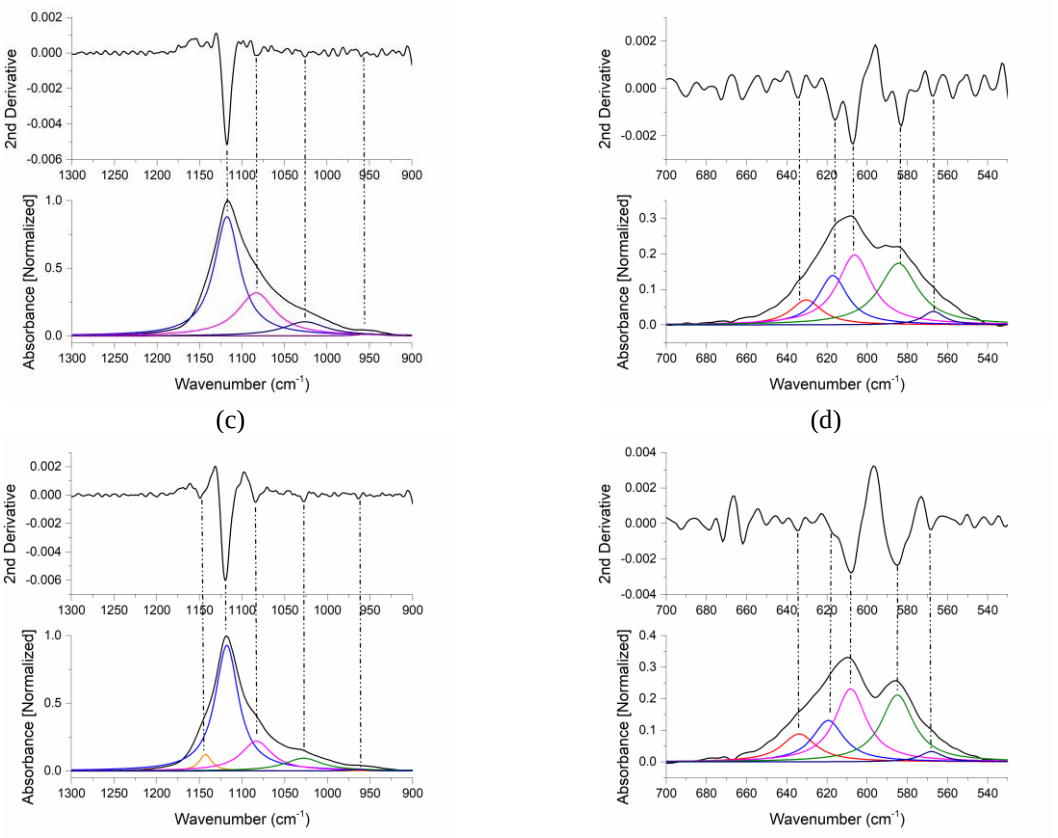

Fig. 4. Deconvoluted FTIR spectra of the CaP/Ti layers at: (a, b) 25 °C, (c, d) 100 °C, and (e, f) 200 °C substrate temperature in the 1300-900 cm^{-1} (a, c, and e) and 700-500 cm^{-1} (b, d, and f) wavenumber ranges

3.4. X-Ray Photoelectron Spectroscopy

The XPS general spectra are presented in Fig. 5. The chemical elements characteristic for calcium phosphates: Ca, P, and O, were identified.

The Ca 2p and P 2p XPS peaks are presented in Fig. 6. The results indicated that as the substrate temperature is increased, there are some shifts to lower binding energies in the case of the XPS peaks characteristic to Ca $2p_{3/2}$, Ca $2p_{1/2}$, and P 2p. Ca $2p_{3/2}$ peak shifts from higher binding energies, 347.4 eV for the layers deposited without heating the substrate, to lower values: 347.2 eV (100 °C) and 347.0 eV (200 °C). The P 2p XPS peak position shifts from 133.5 eV (for the layers deposited at 25 °C and 100 °C) to 133.1 eV (for the layer deposited at 200 °C). These shifts indicate structural modifications at the layer surface as the layer substrate increases. The observed binding energies are characteristic to CaPs compounds [9]. The FTIR analysis sustain these results.

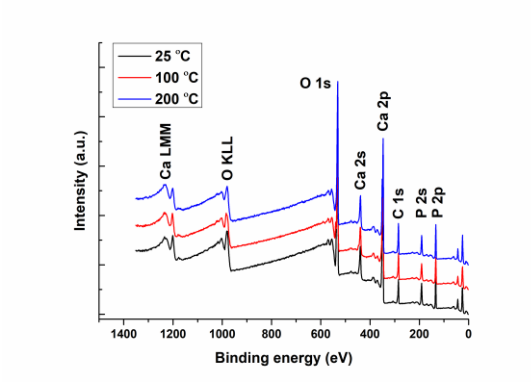

Fig. 5. XPS survey of the CaP/Ti layers.

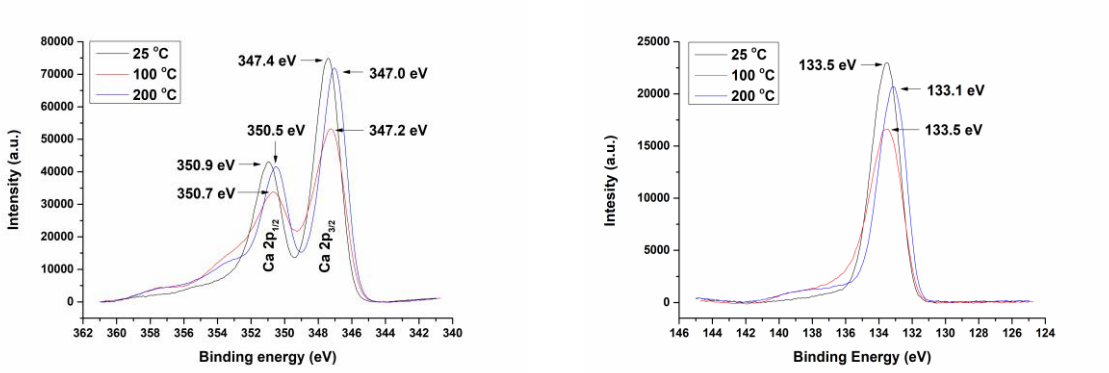

(a) (b)

Fig. 6. XPS peaks of Ca 2p (a) and P 2p (b) for the CaP layers deposited at different substrate temperatures

4. Conclusions

In this study we report the effects of the substrate temperature on the physicochemical properties of calcium phosphates deposited by RF-MS at low power.

The SEM analysis showed that by heating of the substrate during the deposition up to 100 °C and 200 °C, a similar surface morphology can be obtained, while maintaining the same Ca/P atomic ratio of 1.8.

The FTIR spectra showed that as the substrate temperature is increased, the ν_3 band narrows and the ν_4 band splits, indicating a possible modification in the crystalline structure of the films. The begin of HAp structure formation has been evidenced by the presence of absorption bands characteristic to the OH group in the FTIR spectrum of the layer deposited at 200 °C substrate temperature and the decrease of the peak area percentage characteristic to non-apatitic PO_4^{3-}.

These changes were confirmed by the XPS investigation, which showed, by the shifts of the Ca 2p and P 2p peaks, that the surface chemistry of the layers modifies as a function of the substrate temperature.

Considering the increased target-to-substrate distance and the low working power, the results presented in this work are relevant for the development of RF-MS calcium phosphate depositions on heat-sensitive substrates or from composite targets containing organic constituents.

Acknowledgments:

This research was supported by the Romanian Ministry of Research, Innovation and Digitalization under Romanian National Core Program LAPLAS VII—contract no. 30N/2023. We thank Veronica Satulu for XPS measurements.

R E F E R E N C E S

1. Surmenev, R.; Vladescu, A.; Surmeneva, M.; Ivanova, A.; Braic, M.; Grubova, I.; Cotrut, C.M. Radio Frequency Magnetron Sputter Deposition as a Tool for Surface Modification of Medical Implants. In *Modern Technologies for Creating the Thin-film Systems and Coatings*; InTech, 2017 ISBN 978-953-51-3004-8.
2. Surmenev, R.A.; Surmeneva, M.A.; Evdokimov, K.E.; Pichugin, V.F.; Peitsch, T.; Epple, M. The Influence of the Deposition Parameters on the Properties of an Rf-Magnetron-Deposited Nanostructured Calcium Phosphate Coating and a Possible Growth Mechanism. *Surf. Coatings Technol.* **2011**, *205*, 3600–3606, doi:10.1016/j.surfcoat.2010.12.039.
3. Feddes, B.; Vredenberg, A.M.; Wolke, J.G.C.; Jansen, J.A. Bulk Composition of r.f. Magnetron Sputter Deposited Calcium Phosphate Coatings on Different Substrates (Polyethylene, Polytetrafluoroethylene, Silicon). *Surf. Coatings Technol.* **2004**, *185*, 346–355, doi:10.1016/S0257-8972(03)01313-6.
4. López, E.O.; Mello, A.; Sendão, H.; Costa, L.T.; Rossi, A.L.; Ospina, R.O.; Borghi, F.F.; Silva Filho, J.G.; Rossi, A.M. Growth of Crystalline Hydroxyapatite Thin Films at Room Temperature by Tuning the Energy of the RF-Magnetron Sputtering Plasma. *ACS Appl. Mater. Interfaces* **2013**, *5*, 9435–9445, doi:10.1021/am4020007.
5. Zarif, M.E.; Yehia-Alexe, S.A.; Bita, B.; Negut, I.; Locovei, C.; Groza, A. Calcium Phosphates–Chitosan Composite Layers Obtained by Combining Radio-Frequency Magnetron Sputtering and Matrix-Assisted Pulsed Laser Evaporation Techniques. *Polymers (Basel).* **2022**, *14*, 5241, doi:10.3390/polym14235241.
6. Zarif, M.E.; Bita, B.; Yehia-Alexe, S.A.; Negut, I.; Groza, A. Spectral Analysis of Strontium-Doped Calcium Phosphate/Chitosan Composite Films. *Polymers (Basel).* **2023**, *15*, 4245, doi:10.3390/polym15214245.
7. Zarif, M.E.; Bita, B.; Yehia-Alexe, S.A.; Negut, I.; Gradisteanu Pircalabioru, G.; Andronescu, E.; Groza, A. Biological and Physicochemical Analysis of Sr-Doped Hydroxyapatite/Chitosan Composite Layers. *Polymers (Basel).* **2024**, *16*, 1922, doi:10.3390/polym16131922.
8. O'Kane, C.; Duffy, H.; Meenan, B.J.; Boyd, A.R. The Influence of Target Stoichiometry on the Surface Properties of Sputter Deposited Calcium Phosphate Thin Films. *Surf. Coatings Technol.* **2008**, *203*, 121–128, doi:10.1016/j.surfcoat.2008.08.007.
9. Boyd, A.R.; O'Kane, C.; Meenan, B.J. Control of Calcium Phosphate Thin Film Stoichiometry Using Multi-Target Sputter Deposition. *Surf. Coatings Technol.* **2013**, *233*, 131–139,

doi:10.1016/j.surfcoat.2013.04.017.
10. Uskoković, V. Visualizing Different Crystalline States during the Infrared Imaging of Calcium Phosphates. *Vib. Spectrosc.* **2020**, *108*, 103045, doi:10.1016/j.vibspec.2020.103045.
11. Narushima, T.; Ueda, K.; Goto, T.; Masumoto, H.; Katsube, T.; Kawamura, H.; Ouchi, C.; Iguchi, Y. Preparation of Calcium Phosphate Films by Radiofrequency Magnetron Sputtering. *Mater. Trans.* **2005**, *46*, 2246–2252, doi:10.2320/matertrans.46.2246.
12. Ivanova, A.A.; Surmeneva, M.A.; Surmenev, R.A.; Depla, D. Influence of Deposition Conditions on the Composition, Texture and Microstructure of RF-Magnetron Sputter-Deposited Hydroxyapatite Thin Films. *Thin Solid Films* **2015**, *591*, 368–374, doi:10.1016/j.tsf.2015.03.058.
13. Safi, I.N.; Hussein, B.M.A.; Aljudy, H.J.; Tukmachi, M.S. Effects of Long Durations of RF–Magnetron Sputtering Deposition of Hydroxyapatite on Titanium Dental Implants. *Eur. J. Dent.* **2021**, *15*, 440–447, doi:10.1055/s-0040-1721314.
14. Surmeneva, M.A.; Surmenev, R.A.; Chaikina, M. V.; Kachaev, A.A.; Pichugin, V.F.; Epple, M. Phase and Elemental Composition of Silicon-Containing Hydroxyapatite-Based Coatings Fabricated by RF-Magnetron Sputtering for Medical Implants. *Inorg. Mater. Appl. Res.* **2013**, *4*, 227–235, doi:10.1134/S2075113313030131.
15. Ivanova, A.A.; Surmeneva, M.A.; Surmenev, R.A.; Depla, D. Structural Evolution and Growth Mechanisms of RF-Magnetron Sputter-Deposited Hydroxyapatite Thin Films on the Basis of Unified Principles. *Appl. Surf. Sci.* **2017**, *425*, 497–506, doi:10.1016/J.APSUSC.2017.07.039.
16. Pichugin, V.F.; Surmenev, R.A.; Shesterikov, E.V.; Ryabtseva, M.A.; Eshenko, E.V.; Tverdokhlebov, S.I.; Prymak, O.; Epple, M. The Preparation of Calcium Phosphate Coatings on Titanium and Nickel–Titanium by Rf-Magnetron-Sputtered Deposition: Composition, Structure and Micromechanical Properties. *Surf. Coatings Technol.* **2008**, *202*, 3913–3920, doi:10.1016/j.surfcoat.2008.01.038.
17. Bita, B.; Stancu, E.; Stroe, D.; Dumitrache, M.; Ciobanu, S.C.; Iconaru, S.L.; Predoi, D.; Groza, A. The Effects of Electron Beam Irradiation on the Morphological and Physicochemical Properties of Magnesium-Doped Hydroxyapatite/Chitosan Composite Coatings. *Polymers (Basel).* **2022**, *14*, 582, doi:10.3390/polym14030582.
18. Nelea, V.; Morosanu, C.; Iliescu, M.; Mihailescu, I.N. Hydroxyapatite Thin Films Grown by Pulsed Laser Deposition and Radio-Frequency Magnetron Sputtering: Comparative Study. *Appl. Surf. Sci.* **2004**, *228*, 346–356, doi:10.1016/j.apsusc.2004.01.029.
19. Nelea, V.; Morosanu, C.; Iliescu, M.; Mihailescu, I.N. Microstructure and Mechanical Properties of Hydroxyapatite Thin Films Grown by RF Magnetron Sputtering. *Surf. Coatings Technol.* **2003**, *173*, 315–322, doi:10.1016/S0257-8972(03)00729-1.
20. Surmeneva, M.A.; Chaikina, M. V.; Zaikovskiy, V.I.; Pichugin, V.F.; Buck, V.; Prymak, O.; Epple, M.; Surmenev, R.A. The Structure of an RF-Magnetron Sputter-Deposited Silicate-Containing Hydroxyapatite-Based Coating Investigated by High-Resolution Techniques. *Surf. Coatings Technol.* **2013**, *218*, 39–46, doi:10.1016/j.surfcoat.2012.12.023.
21. Groza, A.; Dreghici, D.B.; Ganciu, M. Calcium Phosphate Layers Deposited on Thermal Sensitive Polymer Substrates in Radio Frequency Magnetron Plasma Discharge. *Coatings* **2019**, *9*, 709, doi:10.3390/coatings9110709.
22. Surmenev, R.A.; Ivanova, A.A.; Epple, M.; Pichugin, V.F.; Surmeneva, M.A. Physical Principles of Radio-Frequency Magnetron Sputter Deposition of Calcium-Phosphate-Based Coating with Tailored Properties. *Surf. Coatings Technol.* **2021**, *413*, 127098, doi:10.1016/j.surfcoat.2021.127098.
23. Boyd, A.R.; Rutledge, L.; Randolph, L.D.; Mutreja, I.; Meenan, B.J. The Deposition of Strontium-Substituted Hydroxyapatite Coatings. *J. Mater. Sci. Mater. Med.* **2015**, *26*, 65, doi:10.1007/s10856-014-5377-z.
24. Boyd, A.R.; Meenan, B.J.; Leyland, N.S. Surface Characterisation of the Evolving Nature of

Radio Frequency (RF) Magnetron Sputter Deposited Calcium Phosphate Thin Films after Exposure to Physiological Solution. *Surf. Coatings Technol.* **2006**, *200*, 6002–6013, doi:10.1016/j.surfcoat.2005.09.032.
25. Boyd, A.R.; Rutledge, L.; Randolph, L.D.; Meenan, B.J. Strontium-Substituted Hydroxyapatite Coatings Deposited via a Co-Deposition Sputter Technique. *Mater. Sci. Eng. C* **2015**, *46*, 290–300, doi:10.1016/j.msec.2014.10.046.
26. Ueda, K.; Kawasaki, Y.; Narushima, T.; Goto, T.; Kurihara, J.; Nakagawa, H.; Kawamura, H.; Taira, M. Calcium Phosphate Films with/without Heat Treatments Fabricated Using RF Magnetron Sputtering. *J. Biomech. Sci. Eng.* **2009**, *4*, 392–403, doi:10.1299/jbse.4.392.
27. Feddes, B.; Wolke, J.G.C.; Jansen, J.A.; Vredenberg, A.M. Radio Frequency Magnetron Sputtering Deposition of Calcium Phosphate Coatings: The Effect of Resputtering on the Coating Composition. *J. Appl. Phys.* **2003**, *93*, 9503–9507, doi:10.1063/1.1576894.
28. Goreninskii, S.I.; Bogomolova, N.N.; Malchikhina, A.I.; Golovkin, A.S.; Bolbasov, E.N.; Safronova, T. V.; Putlyaev, V.I.; Tverdokhlebov, S.I. Biological Effect of the Surface Modification of the Fibrous Poly(L-Lactic Acid) Scaffolds by Radio Frequency Magnetron Sputtering of Different Calcium-Phosphate Targets. *Bionanoscience* **2017**, *7*, 50–57, doi:10.1007/s12668-016-0383-x.
29. Surmeneva, M.A.; Surmenev, R.A.; Nikonova, Y.A.; Selezneva, I.I.; Ivanova, A.A.; Putlyaev, V.I.; Prymak, O.; Epple, M. Fabrication, Ultra-Structure Characterization and in Vitro Studies of RF Magnetron Sputter Deposited Nano-Hydroxyapatite Thin Films for Biomedical Applications. *Appl. Surf. Sci.* **2014**, *317*, 172–180, doi:10.1016/j.apsusc.2014.08.104.
30. Berzina-Cimdina, L.; Borodajenko, N. Research of Calcium Phosphates Using Fourier Transform Infrared Spectroscopy. In *Infrared Spectroscopy - Materials Science, Engineering and Technology*; InTech, 2012 ISBN 978-953-51-0537-4.
31. Coates, J. Interpretation of Infrared Spectra, A Practical Approach. In *Encyclopedia of Analytical Chemistry*; John Wiley & Sons, Ltd: Chichester, UK, 2006.
32. Nyquist, R.A.; Kagel, R.O. INFRARED SPECTRA OF INORGANIC COMPOUNDS. In *Handbook of Infrared and Raman Spectra of Inorganic Compounds and Organic Salts*; Elsevier, 1971; Vol. 14, pp. 1–18 ISBN 9780125234504.
33. Lin-Vien, D.; Colthup, N.B.; Fateley, W.G.; Grasselli, J.G. Organophosphorus Compounds. In *The Handbook of Infrared and Raman Characteristic Frequencies of Organic Molecules*; Elsevier, 1991; pp. 263–276.
34. Copete, H.; López, E.; Baudin, C. Synthesis and Characterization of B-Type Carbonated Hydroxyapatite Materials: Effect of Carbonate Content on Mechanical Strength and in Vitro Degradation. *Bol. la Soc. Esp. Ceram. y Vidr.* **2024**, *63*, 255–267, doi:10.1016/j.bsecv.2023.12.001.
35. Lafon, J.P.; Champion, E.; Bernache-Assollant, D. Processing of AB-Type Carbonated Hydroxyapatite Ca10-x(PO4)6-x(CO3)x(OH)2-x-2y(CO3)y Ceramics with Controlled Composition. *J. Eur. Ceram. Soc.* **2008**, *28*, 139–147, doi:10.1016/j.jeurceramsoc.2007.06.009.
36. Prekajski, M.; Mirković, M.; Todorović, B.; Matković, A.; Marinović-Cincović, M.; Luković, J.; Matović, B. Ouzo Effect-New Simple Nanoemulsion Method for Synthesis of Strontium Hydroxyapatite Nanospheres. *J. Eur. Ceram. Soc.* **2016**, *36*, 1293–1298, doi:10.1016/j.jeurceramsoc.2015.11.045.
37. Motisuke, M.; Carrodeguas, R.G.; Zavaglia, C.A. de C. Si-Tricalcium Phosphate Cement: Preparation, Characterization and Bioactivity in SBF. *Mater. Res.* **2011**, *14*, 493–498, doi:10.1590/S1516-14392011005000065.
38. Leon, B.; Jansen, J.A. *Thin Calcium Phosphate Coatings for Medical Implants*; León, B., Jansen, J., Eds.; Springer New York: New York, NY, 2009; ISBN 978-0-387-77718-4.
39. Robinson, L.; Salma-Ancane, K.; Stipniece, L.; Meenan, B.J.; Boyd, A.R. The Deposition of

Strontium and Zinc Co-Substituted Hydroxyapatite Coatings. *J. Mater. Sci. Mater. Med.* **2017**, *28*, 51, doi:10.1007/s10856-017-5846-2.
40. Kaygili, O.; Keser, S.; Ates, T.; Kirbag, S.; Yakuphanoglu, F. Dielectric Properties of Calcium Phosphate Ceramics. *Mater. Sci.* **2016**, *22*, 65–69, doi:10.5755/j01.ms.22.1.7222.
41. Markovic, M.; Fowler, B.O.; Tung, M.S. Preparation and Comprehensive Characterization of a Calcium Hydroxyapatite Reference Material. *J. Res. Natl. Inst. Stand. Technol.* **2004**, *109*, 553, doi:10.6028/jres.109.042.
42. Rey, C.; Shimizu, M.; Collins, B.; Glimcher, M.J. Resolution-Enhanced Fourier Transform Infrared Spectroscopy Study of the Environment of Phosphate Ions in the Early Deposits of a Solid Phase of Calcium-Phosphate in Bone and Enamel, and Their Evolution with Age. I: Investigations in Thev 4 PO4 Domain. *Calcif. Tissue Int.* **1990**, *46*, 384–394, doi:10.1007/BF02554969.
43. Vandecandelaere, N.; Rey, C.; Drouet, C. Biomimetic Apatite-Based Biomaterials: On the Critical Impact of Synthesis and Post-Synthesis Parameters. *J. Mater. Sci. Mater. Med.* **2012**, *23*, 2593–2606, doi:10.1007/s10856-012-4719-y.
44. Rey, C.; Combes, C.; Drouet, C.; Sfihi, H.; Barroug, A. Physico-Chemical Properties of Nanocrystalline Apatites: Implications for Biominerals and Biomaterials. *Mater. Sci. Eng. C* **2007**, *27*, 198–205, doi:10.1016/j.msec.2006.05.015.